J. Biochem. **141,** 709–717 (2007)
doi:10.1093/jb/mvm072

Molecular Anatomy of the Alkaliphilic Xylanase from *Bacillus halodurans* C-125

Mamoru Nishimoto[1], Shinya Fushinobu[2], Akimasa Miyanaga[2], Motomitsu Kitaoka[1,*] and Kiyoshi Hayashi[1]

[1]*Enzyme Laboratory, National Food Research Institute, 2-1-12 Kannondai, Tsukuba, Ibaraki 305-8642; and* [2]*Department of Biotechnology, The University of Tokyo, 1-1-1 Yayoi, Bunkyo-ku, Tokyo 113-8657, Japan*

Received February 5, 2007; accepted February 26, 2007; published online March 23, 2007

Two regions in xylanase A from *Bacillus halodurans* C-125 (XynA), an alkaliphilic xylanase, were identified to be responsible for its activity at basic pH by comparing the dissociation constants of the XynA proton donor Glu residue (pK_{e2} and pK_{es2}) with those of xylanase B from *Clostridium stercorarium* F9 (XynB) and their mutants constructed by substituting either Ser137/Asn127 of XynA/XynB or the 4th loop, designed based on the structural difference close to the proton donor. The substitution of XynB at Asn127 into Ser increased pK_{e2} by 0.37. The effect is explained that the positive charge of His126 likely affects the proton donor via Asn127 and a water molecule in XynB, resulting in a decrease in pK_{e2}, whereas such interactions were not observed with Ser. The substitution of XynB at the 4th loop into XynA (XynB Loop4A) increased the pK_{e2} and pK_{es2} values by 0.29 and 0.62, respectively. The effect of the 4th loop in XynA is likely due to a hydrogen bond between Asp199 in the loop and Tyr239, which interacts with both the proton donors Glu195 and Arg204, with flexibility of the loop. Both the mutations independently affected the increases in pK_{e2}.

Key words: family 10 xylanase, pH-activity relationship.

Abbreviations: XynA, xylanase A from *Bacillus halodurans* C-125; XynB, xylanase B from *Clostridium stercorarium* F9; XynT6, xylanase T6 from *Geobacillus stearothermophilus*; *p*NP-X2, *p*-nitrophenyl xylobioside.

Xylanases, enzymes that hydrolyse the β-1,4-xylosyl bonds in xylan, are classified mainly into the glycoside hydrolase families 10 and 11 (GH10 and GH11), based on their amino acid sequence similarity (*1*). GH10 xylanase A from alkaliphilic *Bacillus halodurans* C-125 (XynA) is an alkaline xylanase because it has a wide range of pH optima, *e.g.* pH 5.8–8.8 in the hydrolysis of *p*-nitrophenyl xylobioside (pNP-X_2) (*2*). This property makes XynA useful in the paper industry, as it can be used instead of toxic chlorinated species to remove lignin from kraft pulp (*3*). Therefore, it is important to understand the mechanism responsible for the activity of alkaline xylanases, such as XynA, at basic pH. Generally, the decreases in activity at acidic and basic pH can be explained by protonation of the nucleophile and deprotonation of the proton donor, resulting in a bell-shaped curve for activity versus pH (Fig. 1). Thus, the acid dissociation constant of the proton donor residue in XynA should be higher than those of normal xylanases.

The acid dissociation constants of catalytic residues are strongly affected by topologically neighbouring amino acid residues. For example, in *Streptomyces lividans* xylanase A (GH10), mutation of Asn127, which is close to the catalytic centre, to Asp decreased pK_{es1} from 4.9 to 4.1 and pK_{es2} from 9.4 to 9.0 (*4*). Moreover, both pK_{e1} and pK_{e2} of GH11 xylanase from *Bacillus cereus* were reduced by mutation of Asn35, which is near the active site, to Asp (*5*), and deletion of the salt bridge located 15 Å from the catalytic residue increased pK_{es1} and pK_{es2} of GH11 xylanase from *Streptomyces* sp (*6*). These results led to the identification of regions in XynA that keep the pK_a of the proton donor high, which could lead to the design of other mutant enzymes active at basic pH.

The 3D structure of GH10 xylanases shows that they consist of a TIM barrel (*7–11*), with their catalytic amino acid residues, a nucleophile and a proton donor, being two glutamic acid residues (*12*, *13*). In addition to the catalytic residues, several amino acid residues are widely conserved, forming subsite −2 to +1 (*14–16*). The roles of some of the amino acid residues around the active cleft have been determined by mutational and structural analyses (*17–21*).

To identify the regions of XynA important for activity at basic pH, we compared the pK_e values with xylanase B from *Clostridium stercorarium* F9 (XynB), which shared 55% amino acid identity with XynA. The pK_{es2} value of XynB (7.82) was much smaller than that of XynA (9.39), whereas both shared similar pK_{es1} values (XynA, 4.10; XynB, 3.86) (*22*). Then, amino acid sequences of XynA and XynB were subdivided into four at highly homologous regions present in their primary structures (Fig. 2): an amino-terminal region (A), a region containing the putative proton donor (P), a region containing the

*To whom correspondence should be addressed. Tel: +81-29-838-8071, Fax: +81-29-838-7321, E-mail: mkitaoka@affrc.go.jp

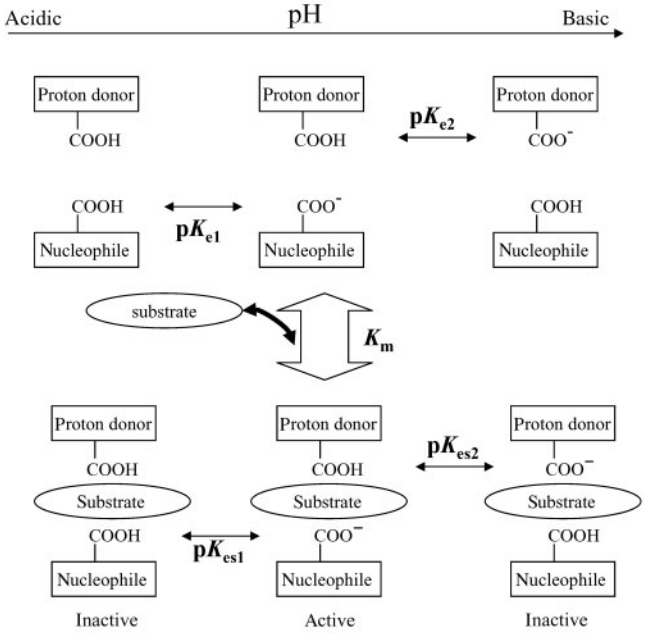

Fig. 1. **Model of the dissociation patterns of an enzyme containing two catalytic acidic residues with substrate binding.** pK_{e1}, pK_a for the nucleophile without substrate; pK_{e2}, pK_a for the proton donor without substrate; pK_{es1}, pK_a for the nucleophile with substrate binding; pK_{es2}, pK_a for the proton donor with substrate binding. The differences in acid dissociation constant before and after substrate binding, $(pK_{es1}-pK_{e1})$ and $(pK_{es2}-pK_{e2})$, are defined as Δ_1 and Δ_2, respectively.

putative catalytic nucleophile (N) and a carboxyl-terminal region (C). Chimeric xylanases were constructed by selective substitution of the four fragments and two of them were found as active as the parental enzymes. The pK_{es2} of chimera 1 ('A' from XynA) and chimera 2 ('A' and 'P' from XynA) were 8.50 and 9.10, respectively, higher than that of XynB (*22*). We also found that a conserved arginine residue, located 4 Å from the proton donor residue, affected the acid dissociation constant during substrate binding, because replacement of this residue with glutamic acid, glutamine or lysine in XynA and XynB markedly decreased their pK_{es2} and Δ_2 (see Fig. 1 for the definition) became negative (*23*). In the present study, we determined the crystal structure of XynB, and compared it with the modelled structure of XynA. Mutant enzymes around the proton donor were analysed to identify the region responsible for the activity of XynA at basic pH.

MATERIALS AND METHODS

Crystallography of XynB and Construction of Model Structure for XynA—Crystallization and X-ray data collection of the mature part of wild-type XynB (from Ala41 to Glu388) have been reported previously (*24*). The crystal belongs to the space group $P2_12_12_1$, with unit-cell parameters $a=64.76$, $b=96.60$, $c=138.44$ Å, and diffracted to 1.8 Å resolution with a Rigaku R-AXIS IV^{++} system. The X-ray data collection statistics have been reported previously (*24*). Initial phases were obtained by the molecular replacement method, using the structure of the extracellular alkaline-tolerant xylanase (XynT6) from *Geobacillus stearothermophilus* T-6 (*25*) (Protein Data Bank code 1HIZ) as a search model. Molecular replacement was performed with MOLREP (*26*) in the CCP4 program suite (*27*). The program ARP/wARP (*28*) was used for automatic model building. Visual inspection of the models was performed using XtalView (*29*). Crystallographic refinement was carried out using CNS 1.1 (Table 1) (*30*). The quality of the present model is good, with all residues being in their most favourable (89.3%), additionally allowed (10.2%) or generously allowed (0.5%) regions of the Ramachandran plot. LSQMAN (*31*) was used for superposition. The coordinates and structure factors have been deposited in the RCSB Protein Data Bank with the accession code 2DEP. The predicted structure of the 4th loop of XynA was constructed by mutating residues of the 4th loop of the crystal structure of XynT6. The positions were refined by 50 steps of energy minimization using CNS 1.1. The figures were prepared using ESpript (*32*), Raster3D (*33*), Molscript (*34*), XtalView and PyMol (*35*).

Preparation of Mutant Enzymes—Polymerase chain reaction (PCR) was performed using KOD-Plus polymerase (Toyobo, Osaka, Japan) and oligonucleotide primers (Table 2). The plasmids prepared previously were used as template DNAs for XynA and XynB (*22*). To prepare mutations, an *Aat*II recognition site was introduced at the 5′ end of the 4th loop in XynB by silent mutation using the mega-primer PCR method (*36*). Megaprimers were prepared for amplification using the mutation primer and pET upstream primer (5′-agatctcgatcccgc gaaat-3′). Second-round PCR was performed using the amplified megaprimer and T7 terminator primer (5′-ctagttattgctcagcgg-3′). The PCR product was ligated into the pET28 vector (Novagen, Darmstadt, Germany) at the *Nco*I/*Xho*I sites using a Ligation High DNA ligation kit (Toyobo). XynA mutants, XynB N127S and XynB L4-3 were also prepared using the mega-primer PCR method. XynB L4-1 and -2 were prepared using the two oligonucleotides shown in Table 2. These two oligonucleotides, with *Aat*II and *Kpn*I sites, were inserted into the XynB plasmid directly after annealing for 5 min at 50°C. The other mutants were constructed by the cassette method. PCR products amplified using each set of mutation primers and pET upstream/T7 terminator primer were ligated into the *Nco*I and *Kpn*I or *Aat*II and *Xho*I sites of each plasmid. All plasmids were designed to add a histidine tag sequence at the carboxyl terminus of the mutated enzyme to facilitate purification. Plasmid DNA was used to transform *Escherichia coli* BL21 (DE3) after sequence confirmation.

Production and Purification of Recombinant Xylanases—Each transformant was cultivated at 30°C with shaking in LB medium, containing 50 μg/ml kanamycin, until the absorbance at 600 nm reached 0.5. Protein expression was induced by addition of isopropyl-1-thio-β-D-galactoside at a final concentration of 0.5 mM, followed by incubation with shaking for an additional 20 h at 30°C. Cells were harvested by centrifugation at 15,000 × *g* for 10 min, resuspended in

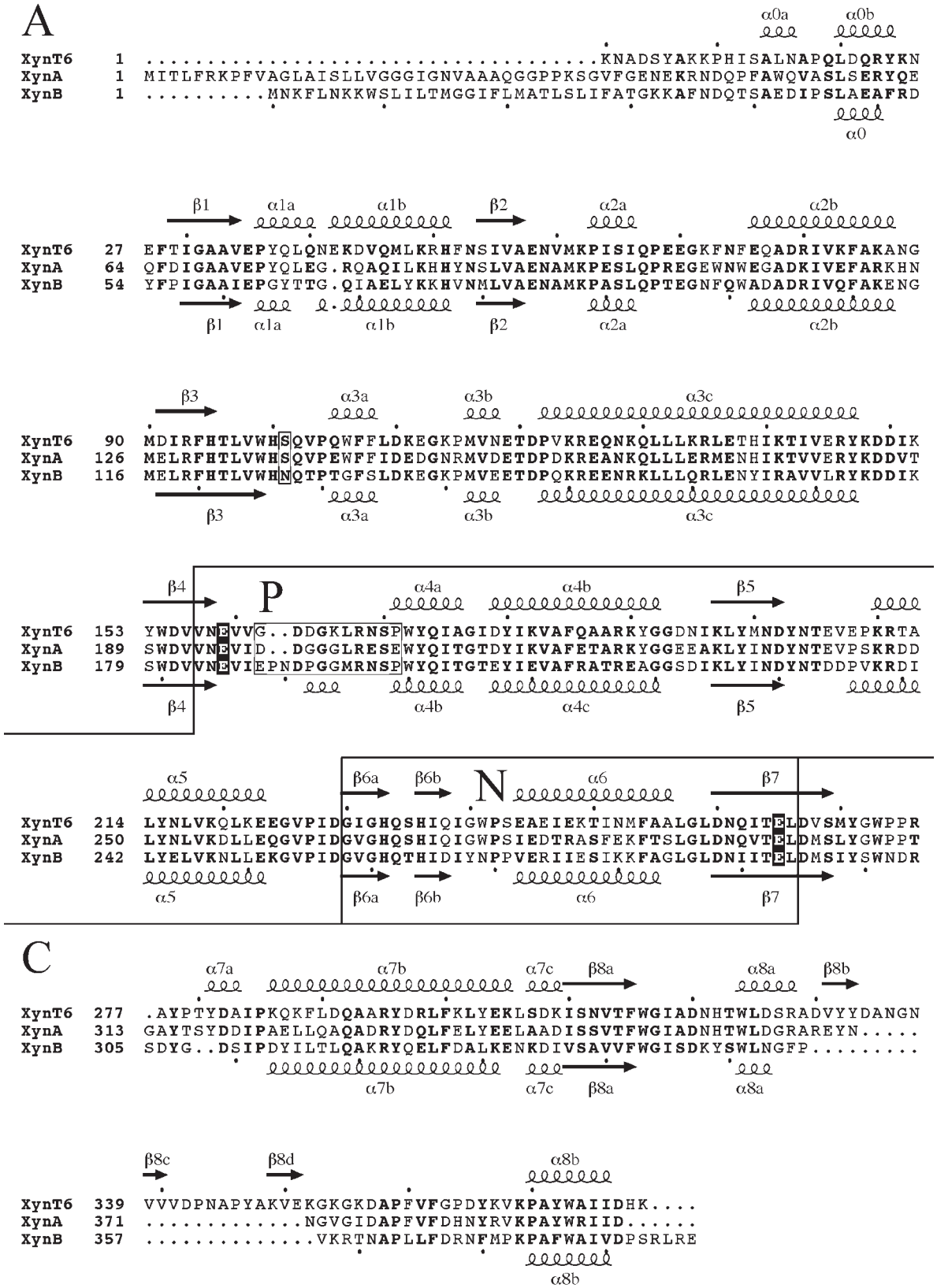

Fig. 2. **Alignment of the amino acid sequences of XynT6, XynA and XynB.** The putative proton donor and catalytic nucleophile residues are shown in reversed shading. Asn127/Ser137 and the 4th loop are boxed. Conserved residues are shown in bold. The secondary structures and their designations are indicated above XynT6 and below XynB. The four regions investigated in our previous study (A, P, N and C) (*22*) are indicated.

20 mM sodium phosphate buffer (pH 7.0), and sonicated using a sonifier (Branson Ultrasonic Corporation, Danbury, CT), with the cell debris removed by centrifugation at $17{,}000 \times g$ for 30 min. Each enzyme was purified from cell-free extract using an AKTA purifier (Pharmacia Biotech, Uppsala, Sweden) with Ni-NTA agarose (Qiagen, Hilden, Germany) and DEAE-Toyopearl (Tosoh, Tokyo) column chromatography, as described (*2*). The homogeneity of the purified enzymes was confirmed by SDS–PAGE (*37*). Protein concentrations were determined using theoretical extinction coefficients calculated from the amino acid sequences of the proteins (*38*). The extinction coefficients values calculated for the XynA and XynB mutants were 91,320 and 77,390/M/cm at 280 nm, respectively.

Measurement of Enzyme Activity and Calculation of Acid Dissociation Constant—Xylanase activity was determined by measuring the amount of *p*-nitrophenol liberated from the substrate *p*NP-X_2 (*39*). Reactions were performed at 40°C in 50 mM MES buffer (pH 6.6) containing 0.01% Triton X-100 and 1.3 mM *p*NP-X_2 and stopped by addition of an equal volume of 1 M sodium carbonate solution. The amount of *p*-nitrophenol generated was quantified by measuring the absorbance at 400 nm. One unit of xylanase activity was defined as the amount of enzyme that liberated 1 μmol of *p*-nitrophenol per min under these conditions. To investigate the relationships between pH and enzyme activity, the enzymatic hydrolyses of *p*NP-X_2 at various concentrations (0.038–1.14 mM) were carried out in 100 mM of each of the following buffers, all of which contained 0.01% Triton X-100, at the pH levels indicated: citrate (pH 3.2 and 3.7), acetate (pH 3.9, 4.3, 4.8, 5.3 and 5.8), MES (pH 5.2, 5.6, 6.1 and 6.6), HEPES (pH 6.5, 6.9, 7.3, 7.8 and 8.3) and CHES buffer (pH 7.7, 8.2, 8.8, 9.2 and 9.7). The kinetic parameters, pK_{es} and pK_e, were calculated by fitting the experimental data to the Michaelis–Menten equation (Eq. 1) and the bell-shaped curves (Eqs 2, 3; see Fig. 1 for the parameters) (*40*) using the GraFit computer program (*41*).

$$v = k_{cat}[E][S]/(K_m + [S])$$

$$V_{max}(pH) = V_{max}/((10^{(pK_{es1}-pH)} + 1)(10^{(pH-pK_{es2})} + 1))$$

$$V_{max}/K_m(pH) = (V_{max}/K_m)/((10^{(pK_{e1}+pH)} + 1)(10^{(pH-pK_{e2})}))$$

The differences in acid dissociation constant before and after substrate binding, (pK_{es1} − pK_{e1}) and (pK_{es2} − pK_{e2}), were defined as Δ_1 and Δ_2, respectively.

Table 1. **Crystallographic refinement statistics.**

Resolution (Å)	50.14–1.80
R/R_{free}[a] (%)	18.4/21.0
No. of protein atoms[b]	5543
No. of water atoms	708
RMSD from ideal values	
Bond length (Å)	0.005
Bond angles (degree)	1.3
Coordinate error (Å)	0.18

[a] Calculated using a test data set containing 5% of the total data selected at random from the observed reflections.
[b] Two molecules in asymmetric unit.

RESULTS AND DISCUSSION

Crystal Structure of XynB—The XynB crystal contained two protein molecules per asymmetric unit, which are related through a non-crystallographic two-fold axis. The structure was solved by molecular replacement using the XynT6 structure as a search model. The final refined model of the structure of XynB contains residues Asp43–Pro382 of molecule A, Ile44–Asp381 of molecule B and 708 water molecules. The two molecules had similar structures throughut the polypeptide. Root mean square deviations for Cα and all atoms between residues 44 and 381 (XynB numbering) were 0.245 and 0.891 Å, respectively. Therefore, our descriptions are mainly for molecule A, unless otherwise noted. The XynB structure was very similar to that of XynT6, as expected from the high degree of amino acid sequence similarity (56% identity). The root mean square deviation between XynB and XynT6 was 0.909 Å for 318 residues. The additional 'subdomain' with three antiparallel β-strands (β8b, β8c and β8d) in the C-terminal region (Asp330–Lys352) of XynT6 (*25*) was deleted in XynB. Compared with XynT6, XynB has an insertion of two residues in the loop connecting β-strand 4 and α-helix 4 (4th loop, Fig. 2). The conformation of the 4th loop was determined unambiguously (Fig. 3). The main-chain trace of the N-terminal half of the 4th loop (Pro189–Gly193) shows significant deviation from that of XynT6 (Asp163–Gly165) due to the insertion of

Table 2. **Primer sequences.**

Mutant	Sequence (5' → 3')
*Aat*II silent	tcatgggacgtcgtgaatgaggtaattga
XynA S137N	ctcgtttggcacaaccaagtaccagaa
XynA Loop4B	acttcatgggacgtcgtcaatgaagttattgaacccaatgatcccg
	gcggtatgagaaacagtccttggtatcaaataacaggtaccgactacatt
XynB N127S	gtgtggcatagtcagacgcccgac
XynB Loop4A	cgtgaatgaggtaattgacgatggcgggggcctgcgtgaatcggaatggtatcagattaccggtac
	cggtaatctgataccattccgattcacgcaggcccccgccatcgtcaattacctcattcacgacgt
XynB Loop4A-1	cgtgaatgaggtaattgacgatggcgggggcatgagaaacagtccttggtatcagattaccggtac
	cggtaatctgataccaaggactgtttctcatgcccccgccatcgtcaattacctcattcacgacgt
XynB Loop4A-2	cgtgaatgaggtaattgaacccaatgatcccggcggtctgcgtgaatcggaatggtatcagattaccggtac
	cggtaatctgataccattccgattcacgcagaccgccgggatcattgggttcaattacctcattcacgacg
XynB Loop4A-3	gtactcggtaccggtaatctgataccattccgagttacgcatgcccccgc

two residues, and this region adopts a short helical conformation. In contrast, there was almost no deviation between the C-terminal half of the 4th loops of XynB and XynT6. The main chain and side chain atoms of Arg196 in XynB also overlapped with those of Arg168 in XynT6. We previously reported that this conserved arginine residue increases pK_{es2}, because it was thought to clamp the proton donor residue and subsite +1 to prevent structural changes during substrate binding (*23*). The results of the present crystallographic study allowed determination of the conformation of the 4th loop of XynB, which had been difficult to predict from the XynT6 structure due to the insertion of two residues. Since the length of the 4th loop of XynA was the same as that of XynT6, we constructed a model of XynA based on the crystal structure of XynT6.

Structural Comparison of XynA and XynB—Two notable differences were found between the structures around the proton donor residues of XynA and XynB, Glu195 (XynA) and Glu185 (XynB) (Fig. 4). Ser137 in XynA, which is located in the 3rd loop and connects β-strand 3 and α-helix 3, is Asn127 in XynB. The side chain of Asn127 in XynB points to the proton donor residue Glu185, but the side chain of Ser137 in XynA, which was modelled based on Ser101 in XynT6, adopts a different conformation. Another difference was found in the structure of the 4th loop due to their low level of sequence similarity (Fig. 2). To study the effects of these differences on activity, six mutant enzymes were prepared: XynA S137N, XynA Loop4B, XynA S137N + Loop4B, XynB N127S, XynB Loop4A and XynB N127S + Loop4A (Fig. 5). The levels of activity of all the mutants were comparable to those of the wild-type enzymes (Table 3).

Effects of the Mutation at Ser137(XynA)/Asn127(XynB)—The acid dissociation constants of the nucleophiles of all the mutant enzymes were about the same as those of their respective parent enzymes, in both the presence and absence of substrate (Table 3). These results suggest that these mutations did not affect the nucleophile. In contrast, the pK_{e2} and pK_{es2} values of XynB N127S were higher than those of XynB by 0.37 and 0.34, respectively. Since the reverse mutations for XynA (XynA S137N) decreased both pK_{e2} and pK_{es2}, Ser137 in XynA was confirmed as one of the factors responsible for maintaining a high pK_{e2} value.

The pK_{e2} value of XynB N127S (7.99) was identical to that of chimera 1 (7.98) (*22*), suggesting that the single mutation is responsible for the effect of the A region (substitution from the N-terminus to Val192; Fig. 2) on the increase in pK_{e2}. In contrast, the Δ_2 value of XynB N127S (0.17) was identical to that of XynB (0.20), whereas chimera 1 had a much larger Δ_2 of 0.52. Thus, another part of the A region must be responsible for the increase in Δ_2 value, the size of the increase in the acid dissociation constant of the proton donor during substrate binding.

In the crystal structure of XynB and the predicted structure of XynA, the side chain of Asn127 (Nδ2) and Ser137 (Cβ) was located 4.4 and 5.2 Å from the Oε1 of their corresponding proton donor residues. Due to the distance separating them, this replacement is not likely to directly affect dissociation of the proton donor. In both enzymes, these residues are neighboured by Trp125 and His126 (numbered according to XynB), both of which are conserved among GH10 xylanases (*9*). In the XynB structure, the distance between Nε2 of His126 and Oδ1 of Asn127 is 3.5 Å, suggesting that these residues interact weakly. A water molecule (Wat519) may form hydrogen bonds with both Asn127 (3.0 Å from Nδ2) and the proton donor Glu185 (2.8 Å from Oε2). Thus, the positive charge of His126 may indirectly affect Glu185

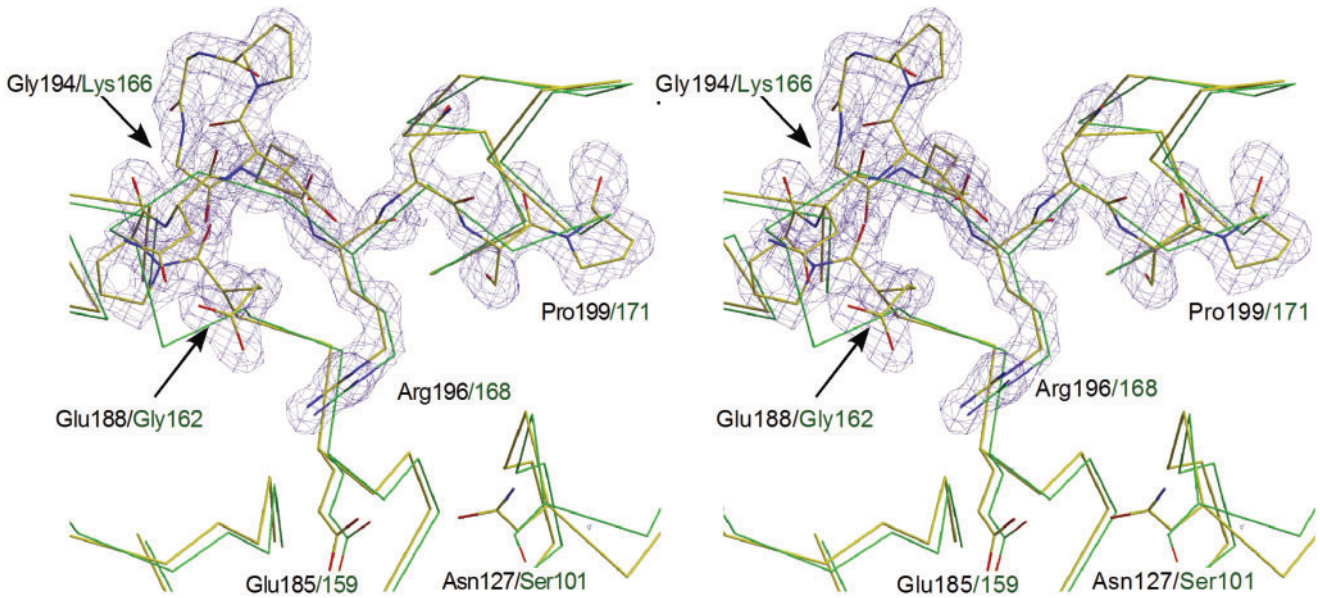

Fig. 3. **Stereoview of superposition of the structure of XynB (yellow) and XynT6 (green).** The electron density map around the 4th loop of the XynB crystal structure is shown. Residue names and numbers are given in the order of XynB/XynT6. Residues flanking the deviated region are indicated by arrows.

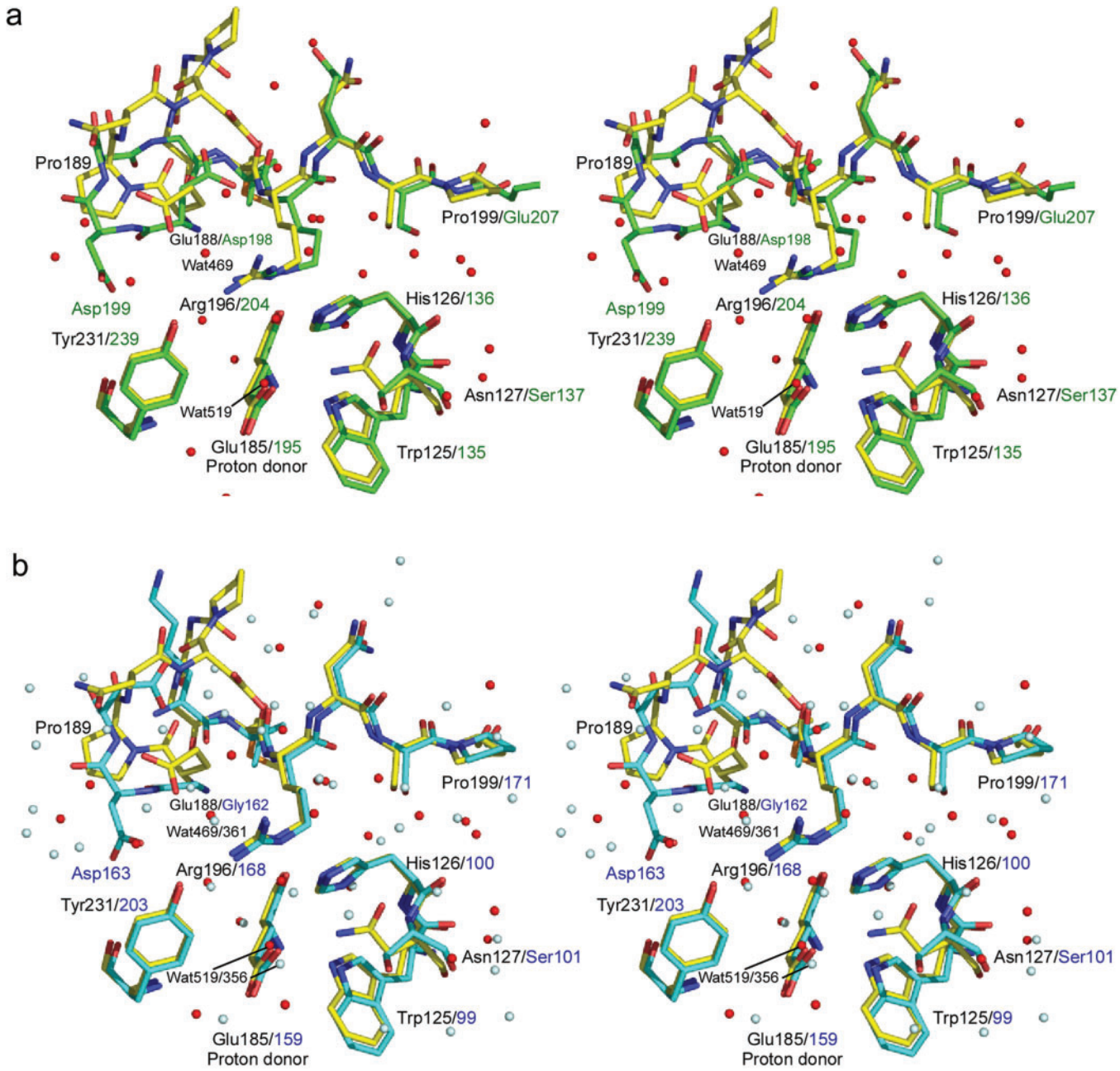

Fig. 4. **Stereoview of superposition of the crystal structure of XynB (yellow) and the predicted structure of XynA (green) (a), and the structure of XynB (yellow) and XynT6 (pale cyan) (b) around the proton donor residue.** Water molecules of XynB and XynT6 are coloured red and cyan, respectively. Residue names and numbers are labelled in the order XynB/XynA (a) and XynB/XynT6 (b).

through Asn127 and Wat519, resulting in a decrease in pK_{e2}.

In contrast, the Ser101 residue of XynT6 (corresponding to Ser137 of XynA) likely does not interact with His100. Although Wat356, which forms a hydrogen bond with the proton donor Glu159, is located at a similar position (Wat519 in XynB), it is far from Ser101, making it unlikely that His100 interacts with Glu159 in XynT6. Because these residues are conserved by both XynT6 and XynA, His136 probably does not affect the XynA proton donor Glu195, thus causing no decrease in pK_{e2}.

Effects of the Substitution of the 4th Loop—The substitution of XynB at the 4th loop into XynA (XynB Loop4A) increased the pK_{e2} and pK_{es2} values by 0.29 and 0.62, respectively. The pK_{e2} and pK_{es2} values of the reverse mutant, XynA Loop4B, were smaller than those of XynA by 0.32 and 0.63, respectively, suggesting that the 4th loop also plays a role in controlling activity at basic pH. The double mutations showed a cooperative

effect. The pK_{e2} value of XynB N127S + Loop4A was 0.58 higher than that of XynB, close to the sum of the effects of both single mutations alone (0.37 + 0.29). The same effect was also observed with XynA S137N + Loop4B. Thus, Ser137 and the 4th loop independently increased the pK_a value of the proton donor.

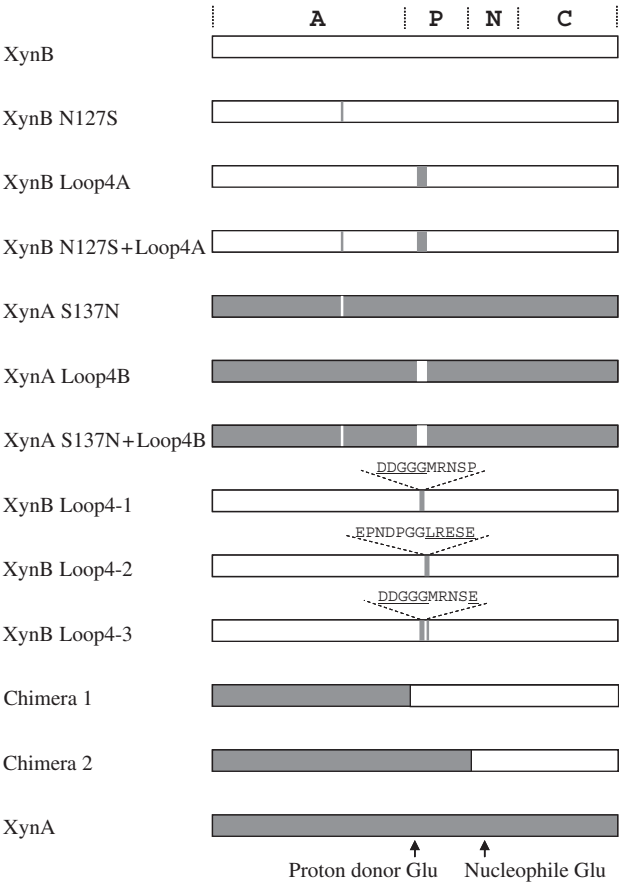

Fig. 5. **Schematic diagram of the primary structures of mutated xylanases.** White and gray boxes are derived from XynB and XynA, respectively. The letters A, P, N and C indicate the division in chimeric xylanases described in our previous report (*22*).

The pK_{e2} values of XynB N127S + Loop4A and chimera 2 were identical, 8.20 and 8.19, respectively. The factors responsible for the increase in pK_{e2} in chimera 2 can be explained completely by N127S mutation and replacement of the 4th loop in XynA. The Δ_2 values of XynB N127S + Loop4A and chimera 2 were 0.62 and 0.91, respectively, with the difference, 0.29, similar to that between XynB N127S and chimera 1 (0.35). This finding suggests that the increases in pK_{e2} and Δ_2 observed when the P region (from Val193 to Asp265, Fig. 5) in chimera 2 was replaced were only due to the replacement of the 4th loop. The reason for the pK_{e2} difference of 0.29 between XynB N127S + Loop4A (8.20) and wild-type XynA (8.49) has yet to be determined, indicating that other areas in the N or C regions are responsible for the remainder of the increase in pK_{e2}.

Mechanism of the Effect of the 4th Loop—To identify the amino acid residues in the 4th loop responsible for the activity at basic pH, we generated two XynB-based mutants: XynB Loop4A-1, in which the N-terminal half of the 4th loop was replaced with that of XynA; and XynB Loop4A-2, in which the C-terminal half of the 4th loop was replaced with that of XynA (Fig. 5). The pK_{e2} value of XynB Loop4A-1 was 7.90, which was identical to that of XynB Loop4A (7.91), whereas that of XynB was 7.62. However, the Δ_2 value of XynB Loop4A-1 (0.18) was identical to that of XynB (0.20). These results suggest that the N-terminal half of the 4th loop of XynA alone was responsible for the increase in the acid dissociation constant of the proton donor in the absence of substrate, but does not participate in its increase during substrate binding.

This region of XynA contains a negatively charged aspartic acid residue (Asp199), whereas there is no corresponding residue in XynB (Fig. 4). However, the distance between Asp199 and Glu195 (proton donor) is 8.4 Å (Oδ1 of Asp199 to Cδ of Glu195), indicating that Asp199 does not affect the proton donor directly. No water molecule was found to interact with both Asp199 and Glu195. Arg204, which is located between Asp199 and Glu195, likely does not play a mediating role, because substitution of Arg204 did not affect pK_{e2} (*23*). The effect of Asp199 can be explained by the formation of a hydrogen bond between this residue and Tyr239 (2.7 Å,

Table 3. **The k_{cat} values and acid dissociation constants for wild-type and mutated xylanases.**

	k_{cat} (s^{-1})	pK_{e1}	pK_{es1}	Δ_1	pK_{e2}	pK_{es2}	Δ_2
XynB[a]	58.1 ± 0.7	4.23 ± 0.09	3.86 ± 0.09	−0.37	7.62 ± 0.09	7.82 ± 0.08	0.20
XynB N127S	53.7 ± 0.7	4.26 ± 0.09	3.82 ± 0.08	−0.44	7.99 ± 0.07	8.16 ± 0.06	0.17
XynB Loop4A	46.2 ± 0.2	4.36 ± 0.08	3.79 ± 0.09	−0.57	7.91 ± 0.07	8.44 ± 0.06	0.53
XynB N127S + Loop4A	34.4 ± 0.3	4.44 ± 0.11	3.94 ± 0.06	−0.50	8.20 ± 0.09	8.82 ± 0.05	0.62
XynA S137N	33.5 ± 0.6	4.70 ± 0.10	4.23 ± 0.06	−0.47	8.36 ± 0.08	9.05 ± 0.07	0.69
XynA Loop4B	32.6 ± 0.5	4.63 ± 0.09	4.28 ± 0.08	−0.35	8.17 ± 0.08	8.76 ± 0.08	0.59
XynA S137N + Loop4B	31.3 ± 0.9	4.61 ± 0.09	4.29 ± 0.06	−0.32	8.03 ± 0.08	8.48 ± 0.06	0.45
XynB Loop4A-1	58.1 ± 0.4	4.35 ± 0.08	3.92 ± 0.07	−0.43	7.90 ± 0.07	8.08 ± 0.07	0.18
XynB Loop4A-2	52.7 ± 0.4	4.16 ± 0.07	3.93 ± 0.06	−0.23	7.83 ± 0.07	7.98 ± 0.05	0.15
XynB Loop4A-3	54.4 ± 0.7	4.39 ± 0.08	3.90 ± 0.07	−0.49	7.89 ± 0.07	8.37 ± 0.06	0.48
Chimera 1[a]	38.2 ± 0.4	4.73 ± 0.11	4.17 ± 0.12	−0.56	7.98 ± 0.09	8.50 ± 0.10	0.52
Chimera 2[a]	40.3 ± 0.5	4.83 ± 0.11	4.27 ± 0.09	−0.56	8.19 ± 0.10	9.10 ± 0.03	0.91
XynA[a]	32.4 ± 0.4	4.72 ± 0.21	4.10 ± 0.08	−0.62	8.49 ± 0.18	9.39 ± 0.08	0.90

[a]Derived from reference (*22*).

Oε1 of Asp199 to OH of Tyr 239) and the close location of Tyr 239 and Glu195 (3.5 Å, Tyr239 Cδ2 to Glu195 Oε2).

The Δ_2 value of XynB Loop4A-2 did not differ much from that of XynB, suggesting that this region does not affect the Δ_2 value directly. Thus, the N-terminal half of the 4th loop must act in concert with its C-terminal half in increasing the Δ_2 value. We prepared XynB-based mutant, XynB Loop4A-3, in which the proline residue at the loop end of XynB Loop4A-1 was replaced with the glutamic acid residue in XynA (Fig. 3), and found that its pK_{e2} and Δ_2 values were identical to those of XynB Loop4A. A comparison of XynB Loop4A-1 and XynB Loop4A-3 suggested that the glutamic acid residue located at the end of the 4th loop, in concert with the N-terminal half of this loop, was necessary to increase the Δ_2 value.

We previously reported that substitution of the conserved arginine residue in the 4th loop of XynA (Arg204) and XynB (Arg196) with several residues had no effect on each pK_{e2} value, but resulted in Δ_2 being similar, around −0.3, in both enzymes, despite the considerable difference in Δ_2 values between native XynA (0.90) and XynB (0.20) (*23*). Thus, the conformation of the arginine residue is responsible for the high Δ_2 value of XynA.

This arginine residue forms a hydrogen bond with a tyrosine residue (Tyr239/231 for XynA/XynB), forming subsite + 1 (*14*) and restricting the conformational change of the 4th loop during substrate binding (*23*). The formation of the hydrogen bond between Asp199 and Tyr239 thus likely affects the conformation of Arg204 through Tyr239 during the substrate binding at subsite +1. A proline residue at the end of the loop would reduce its flexibility, possibly preventing Arg204 from attaining the proper location for substrate binding. A water molecule (Wat469) forms hydrogen bonds with both Glu188 (2.7Å, Oε1) and Arg196 (2.9Å, NH1) in XynB (Fig. 4). The difference in Δ_2 between XynA and XynB is also explainable with these hydrogen bonds, because they likely fix the side chain of Arg196.

This work was supported in part by the Program for Promotion of Basic Research Activities for Innovative Biosciences (PROBRAIN), and the National Project on Protein Structural and Functional Analysis.

REFERENCES

1. Henrissat, B. (1991) A classification of glycosyl hydrolases based on amino acid sequence similarities. *Biochem. J.* **280**, 309–316
2. Nishimoto, M., Honda, Y., Kitaoka, M., and Hayashi, K. (2002) A kinetic study on pH-activity relationship of XynA from alkaliphilic *Bacillus halodurans* C-125 by using aryl-xylobiosides. *J. Biosci. Bioeng.* **93**, 428–430
3. Bissoon, S., Christov, L., and Singh, S. (2002) Bleach boosting effects of purified xylanase from *Thermomyces lanuginosus* SSBP on bagasse pulp. *Process Biochem.* **37**, 567–572
4. Roberge, M., Dupont, C., Morosoli, R., Shareck, F., and Kluepfel, D. (1997) Asparagine-127 of xylanase A from *Streptomyces lividans*, a key residue in glycosyl hydrolases of superfamily 4/7: kinetic evidence for its involvement in stabilization of the catalytic intermediate. *Protein Eng.* **10**, 399–403
5. Joshi, M.D., Sidhu, G., Pot, I., Brayer, G.D., Withers, S.G., and McIntosh, L.P. (2000) Hydrogen bonding and catalysis: a novel explanation for how a single amino acid substitution can change the pH optimum of a glycosidase. *J. Mol. Biol.* **299**, 255–279
6. De Lemos Esteves, F., Gouders, T., Lamotte-Brasseur, J., Rigali, S., and Frere, J.M. (2005) Improving the alkalophilic performances of the Xyl1 xylanase from *Streptomyces* sp. S38: structural comparison and mutational analysis. *Protein Sci.* **14**, 292–302
7. White, A., Withers, S.G., Gilkes, N.R., and Rose, D.R. (1994) Crystal structure of the catalytic domain of the β-1,4-glycanase cex from *Cellulomonas fimi*. *Biochemistry* **33**, 12546–12552
8. Natesh, R., Bhanumoorthy, P., Vithayathil, P.J., Sekar, K., Ramakumar, S., and Viswamitra, M.A. (1999) Crystal structure at 1.8 Å resolution and proposed amino acid sequence of a thermostable xylanase from *Thermoascus aurantiacus*. *J. Mol. Biol.* **288**, 999–1012
9. Harris, G.W., Jenkins, J.A., Connerton, I., Cummings, N., Lo Leggio, L., Scott, M., Hazlewood, G.P., Laurie, J.I., Gilbert, H.J., and Pickersgill, R.W. (1994) Structure of the catalytic core of the family F xylanase from *Pseudomonas fluorescens* and identification of the xylopentaose-binding sites. *Structure* **2**, 1107–1116
10. Fujimoto, Z., Kuno, A., Kaneko, S., Kobayashi, H., Kusakabe, I., and Mizuno, H. (2002) Crystal structures of the sugar complexes of *Streptomyces olivaceoviridis* E-86 xylanase: sugar binding structure of the family 13 carbohydrate binding module. *J. Mol. Biol.* **316**, 65–78
11. Derewenda, U., Swenson, L., Green, R., Wei, Y., Morosoli, R., Shareck, F., Kluepfel, D., and Derewenda, Z.S. (1994) Crystal structure, at 2.6-Å resolution, of the *Streptomyces lividans* xylanase A, a member of the F family of β-1,4-D-glycanases. *J. Biol. Chem.* **269**, 20811–20814
12. MacLeod, A.M., Lindhorst, T., Withers, S.G., and Warren, R.A. (1994) The acid/base catalyst in the exoglucanase/xylanase from *Cellulomonas fimi* is glutamic acid 127: evidence from detailed kinetic studies of mutants. *Biochemistry* **33**, 6371–6376
13. Tull, D., Withers, S.G., Gilkes, N.R., Kilburn, D.G., Warren, R.A., and Aebersold, R. (1991) Glutamic acid 274 is the nucleophile in the active site of a "retaining" exoglucanase from *Cellulomonas fimi*. *J. Biol. Chem.* **266**, 15621–15625
14. Charnock, S.J., Spurway, T.D., Xie, H., Beylot, M.H., Virden, R., Warren, R.A., Hazlewood, G.P., and Gilbert, H.J. (1998) The topology of the substrate binding clefts of glycosyl hydrolase family 10 xylanases are not conserved. *J. Biol. Chem.* **273**, 32187–32199
15. Ducros, V., Charnock, S.J., Derewenda, U., Derewenda, Z.S., Dauter, Z., Dupont, C., Shareck, F., Morosoli, R., Kluepfel, D., and Davies, G.J. (2000) Substrate specificity in glycoside hydrolase family 10. Structural and kinetic analysis of the *Streptomyces lividans* xylanase 10Å. *J. Biol. Chem.* **275**, 23020–23026
16. Leggio, L.L., Jenkins, J., Harris, G.W., and Pickersgill, R.W. (2000) X-ray crystallographic study of xylopentaose binding to *Pseudomonas fluorescens* xylanase A. *Proteins* **41**, 362–373
17. Lo Leggio, L., Kalogiannis, S., Eckert, K., Teixeira, S.C.M., Bhat, M.K., Andrei, C., Pickersgill, R.W., and Larsen, S. (2001) Substrate specificity and subsite mobility in *T. aurantiacus* xylanase 10A. *FEBS Lett.* **509**, 303–308
18. Pell, G., Taylor, E.J., Gloster, T.M., Turkenburg, J.P., Fontes, C.M., Ferreira, L.M., Nagy, T., Clark, S.J.,

Davies, G.J., and Gilbert, H.J. (2004) The mechanisms by which family 10 glycoside hydrolases bind decorated substrates. *J. Biol. Chem.* **279**, 9597–9605
19. Fujimoto, Z., Kaneko, S., Kuno, A., Kobayashi, H., Kusakabe, I., and Mizuno, H. (2004) Crystal structures of decorated xylooligosaccharides bound to a family 10 xylanase from *Streptomyces olivaceoviridis* E-86. *J. Biol. Chem.* **279**, 9606–9614
20. Pell, G., Szabo, L., Charnock, S.J., Xie, H., Gloster, T.M., Davies, G.J., and Gilbert, H.J. (2004) Structural and biochemical analysis of *Cellvibrio japonicus* xylanase 10C: how variation in substrate-binding cleft influences the catalytic profile of family GH-10 xylanases. *J. Biol. Chem.* **279**, 11777–11788
21. Andrews, S.R., Charnock, S.J., Lakey, J.H., Davies, G.J., Claeyssens, M., Nerinckx, W., Underwood, M., Sinnott, M.L., Warren, R.A., and Gilbert, H.J. (2000) Substrate specificity in glycoside hydrolase family 10. Tyrosine 87 and leucine 314 play a pivotal role in discriminating between glucose and xylose binding in the proximal active site of *Pseudomonas cellulosa* xylanase 10A. *J. Biol. Chem.* **275**, 23027–23033
22. Nishimoto, M., Kitaoka, M., and Hayashi, K. (2002) Employing chimeric xylanases to identify regions of an alkaline xylanase participating in enzyme activity at basic pH. *J. Biosci. Bioeng.* **94**, 395–400
23. Nishimoto, M., Kitaoka, M., Fushinobu, S., and Hayashi, K. (2005) The role of conserved arginine residue in loop 4 of glycoside hydrolase family 10 xylanases. *Biosci. Biotechnol. Biochem.* **69**, 904–910
24. Nishimoto, M., Fushinobu, S., Miyanaga, A., Wakagi, T., Shoun, H., Sakka, K., Ohmiya, K., Nirasawa, S., Kitaoka, M., and Hayashi, K. (2004) Crystallization and preliminary X-ray analysis of xylanase B from *Clostridium stercorarium*. *Acta Crystallogr. D Biol. Crystallogr.* **60**, 342–343
25. Teplitsky, A., Mechaly, A., Stojanoff, V., Sainz, G., Golan, G., Feinberg, H., Gilboa, R., Reiland, V., Zolotnitsky, G., Shallom, D., Thompson, A., Shoham, Y., and Shoham, G. (2004) Structure determination of the extracellular xylanase from *Geobacillus stearothermophilus* by selenomethionyl MAD phasing. *Acta Crystallogr. D Biol. Crystallogr.* **60**, 836–848
26. Vagin, A. and Teplyakov, A. (1997) MOLREP: an automated program for molecular replacement. *J. Appl. Crystallogr.* **30**, 1022–1025
27. Collaborative Computational Project Number 4. (1994) The ccp4 suite - programs for protein crystallography. *Acta Crystallogr. D Biol. Crystallogr.* **50**, 760–763
28. Morris, R.J., Perrakis, A., and Lamzin, V.S. (2002) ARP/wARP's model-building algorithms. I. The main chain. *Acta Crystallogr. D Biol. Crystallogr.* **58**, 968–975
29. McRee, D.E. (1999) XtalView Xfit – A versatile program for manipulating atomic coordinates and electron density. *J. Struct. Biol.* **125**, 156–165
30. Brünger, A.T., Adams, P.D., Clore, G.M., DeLano, W.L., Gros, P., Grosse-Kunstleve, R.W., Jiang, J.S., Kuszewski, J., Nilges, M., Pannu, N.S., Read, R.J., Rice, L.M., Simonson, T., and Warren, G.L. (1998) Crystallography & NMR system: a new software suite for macromolecular structure determination. *Acta Crystallogr. D Biol. Crystallogr.* **54**, 905–921
31. Kleywegt, G.J. and Jones, T.A. (1994) A super position. *CCP4/ESF-EACBM Newsletter on Protein Crystallography* **31**, 9–14
32. Gouet, P., Courcelle, E., Stuart, D.I., and Metoz, F. (1999) ESPript: analysis of multiple sequence alignments in PostScript. *Bioinformatics* **15**, 305–308
33. Merritt, E.A. and Bacon, D.J. (1997) Raster3D: Photorealistic molecular graphics. *Methods Enzymol.* **277**, 505–524
34. Kraulis, P.J. (1991) Molscript – a program to produce both detailed and schematic plots of protein structures. *J. Appl. Crystallogr.* **24**, 946–950
35. DeLano, W.L. (2002) *The PyMOL Molecular Graphic System* Delano Scientific, San Carlos, California
36. Ke, S.H. and Madison, E.L. (1997) Rapid and efficient site-directed mutagenesis by single-tube 'megaprimer' PCR method. *Nucleic Acids Res.* **25**, 3371–3372
37. Laemmli, U.K. (1970) Cleavage of structural proteins during the assembly of the head of bacteriophage T4. *Nature* **227**, 680–685
38. Gill, S.C. and von Hippel, P.H. (1989) Calculation of protein extinction coefficients from amino acid sequence data. *Anal. Biochem.* **182**, 319–326
39. Kitaoka, M., Haga, K., Kashiwagi, Y., Sasaki, T., Taniguchi, H., and Kusakabe, I. (1993) Kinetic studies on *p*-nitrophenyl-cellobioside hydrolyzing xylanase from *Cellvibrio gilvus*. *Biosci. Biotechnol. Biochem.* **57**, 1987–1989
40. Dixon, M. (1953) The effect of pH on the affinities of enzymes for substrates and Inhibitors. *Biochem. J.* **55**, 161–170
41. Leatherbarrow, R.J. (1990) Using linear and non-linear regression to fit biochemical data. *Trends Biochem. Sci.* **15**, 455–458